

Optimization of Bit Geometry and Multi-Reader Geometry for Two-Dimensional Magnetic Recording

John R. Barry¹, Bane Vasić², Mehrdad Khatami², Mohsen Bahrami², Yasuaki Nakamura³,
Yoshihiro Okamoto³, and Yasushi Kanai⁴

¹School of Electrical and Computer Engineering, Georgia Institute of Technology, Atlanta, GA 30332-0250 USA

²Department of Electrical and Computer Engineering, University of Arizona, Tucson, AZ 85721 USA

³Graduate School of Science and Engineering, Ehime University, Matsuyama 790-8577, Japan

⁴Department of Information and Electronics Engineering, Niigata Institute of Technology, Kashiwazaki 945-1195, Japan

The move from traditional single-track magnetic recording to two-dimensional magnetic recording (TDMR) with squeezed tracks and multiple readers opens up new design degrees of freedom beyond the track pitch and bit-aspect ratio, including the widths, spacing, and crosstrack positions of the readers. In this paper, we present a systematic method for determining the combination of multi-reader geometry, track pitch, and bit-aspect ratio that maximizes the areal density of a TDMR system using single-track detectors. The method combines realistic modeling of the medium and write/read processes, advanced signal detection, and information-theoretic tools. For the particular head and medium we consider, the two-reader geometry that maximizes areal density with zero skew and zero misregistration was found to use different-sized readers (the smaller having a full-width at half-maximum width, i.e., 96% of the track pitch and the larger having a width, i.e., 148% of the track pitch) with significant overlap in the crosstrack direction (centers spaced by one eighth of the track pitch). The optimal bit-aspect ratio was 2.2. At the optimal operating point, the information rate per coded bit is 0.8.

Index Terms—Data-dependent noise, information theory, intersymbol interference (ISI), intertrack interference (ITI), shingled magnetic recording, two-dimensional magnetic recording (TDMR).

I. INTRODUCTION

TWO-DIMENSIONAL magnetic recording (TDMR) is an accepted part of the industry's technology roadmap for hard disk drives [1]–[3]. The first implementations of TDMR will likely use just two closely spaced stacked readers on tracks written using shingled magnetic recording [4]. The optimization of a conventional single-track recording system is a complex process involving many parameters. The optimization of a dual-reader TDMR system is still more complex involving at least three additional parameters: the two reader widths and the crosstrack offset (or spacing) between the readers.

This paper examines the optimization of a dual-reader TDMR system to maximize customer areal density at a fixed radius and velocity (the change in crosstrack offset as a function of radius/skew for a stacked reader is not dealt with here). The search for the optimum is conducted over the following six parameters: 1) track pitch; 2) channel/media linear density; 3) reader-1 width; 4) reader-2 width; 5) reader-1 position; and 6) reader-2 position.

The optimization is done through software processing of waveforms derived from a quasi-static recording simulation of long pseudorandom bit sequences [5]. An important part of this paper is the testing of the simulated waveforms to see if they exhibit various characteristics of real waveforms. The signal is characterized in two dimensions in terms of its linear and nonlinear responses, its noise spectra, and noise and signal power as a function of crosstrack position.

Manuscript received July 24, 2015; revised August 31, 2015; accepted September 8, 2015. Date of publication September 29, 2015; date of current version January 18, 2016. Corresponding author: J. R. Barry (e-mail: barry@ece.gatech.edu).

Color versions of one or more of the figures in this paper are available online at <http://ieeexplore.ieee.org>.

Digital Object Identifier 10.1109/TMAG.2015.2483593

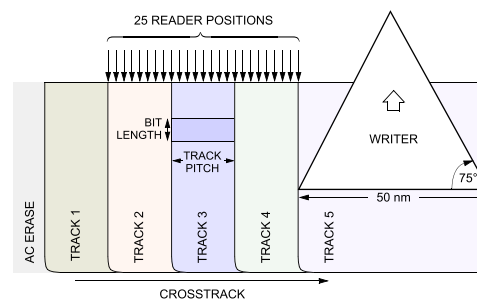


Fig. 1. Geometry of the model, showing the five-shingled tracks and 25 possible reader locations. The physical width of the writer is 50 nm, while the track pitch ranges from 16.1 to 26.1 nm.

The recording medium for the simulations is set at 22 Tgr/in² (about twice today's grain densities), and the components and the magnetic spacing are gauged such as to support a raw channel density of roughly 4 Tb/in².

II. CHANNEL MODEL AND DATABASE

Waveforms are derived from a simulation that uses realistic head fields and a Voronoi medium with Stoner–Wohlfarth switching [6]–[9]. The mean grain pitch is 6 nm, and there are distributions in the anisotropy magnitude and angle. Magnetostatic and exchange interactions are included. The read sensitivity function is obtained by the 3-D finite-element modeling of a double-shielded magnetoresistive reader at several widths.

A database of 1000 oversampled waveforms was created, based on a setting in which five consecutive tracks are written in a shingled fashion, as shown in Fig. 1, each track with independent pseudorandom bit sequences of length 40 950. The center track (track 3) is the track of interest.

A total of 900 readback waveforms were generated with a bit length of 7.3 nm, one for each of six track pitches (from 16.1 to 26.1 nm in 2 nm increments), six reader widths (from 70% to 145% of a nominal reader width; see the following paragraph for clarification), and 25 reader positions (spanning the center three tracks at one eighth of a track increments). The additional 100 readback waveforms were generated at a track pitch of 16.1 nm and 70% reader width, one for each of four additional bit lengths (5.3, 6.3, 8.3, and 9.3 nm) and the same 25 reader positions. All readback waveforms were oversampled (perfect synchronization) at two samples per bit.

All readers have identical downtrack parameters (magnetoresistive (MR) element thickness is 2 nm and spacing between shields is 22 nm), while their crosstrack parameters are scaled relative to the so-called nominal (100%) reader, for which the MR element width is 17 nm, and the spacing between side shields is 30 nm. The full-width at half-maximum (FWHM) of the nominal reader sensitivity function is 20.8 nm. The FWHMs of the 70%, 85%, 115%, 130%, and 145% readers are 15.5, 18.3, 23.8, 26.4, and 29.1 nm, respectively.

The same amount of white and Gaussian electronic noise was added to all readback waveforms having a bit length of 7.3 nm, independent of the reader width, by adding an independent zero-mean Gaussian random variable to each oversampled readback sample, with standard deviation $\sigma_e = 0.04$. This electronic noise can be viewed as arising in the front-end amplifier, after the reader. The signal-to-electronic noise ratio thus loses approximately¹ 6 dB per halving of the reader width. The corresponding power of the added noise within the Nyquist band is 24.6 dB below the saturation (constant response) signal level for the centered 100% width reader at 22.1 nm track pitch, which for that scenario is 10.1% of the total noise power (including media noise).

III. CHANNEL CHARACTERIZATION

The validity of the write and read model described above was tested by characterizing the signal and noise in both the downtrack and crosstrack dimensions, as described in this section. These tests were carried out directly on the readback waveforms produced by the model, using the same methodology that we would apply to spinstand measured waveforms.

Let \mathbf{r} denote the row vector of the more than 80 000 oversampled samples of a given readback waveform; a linear model that accounts for contributions from all five tracks is

$$\mathbf{r} = \sum_{n=1}^5 \mathbf{h}_n \mathbf{A}_n + \mathbf{e}$$

where \mathbf{h}_n is the oversampled linear impulse response from the n th track to the given reader, \mathbf{A}_n is a convolution matrix for the upsampled bits written on the n th track, and \mathbf{e} represents any modeling errors and noise. More compactly, we can

¹The 6 dB is only approximate, because the signal amplitude does not scale linearly with reader width (see Fig. 3); the true SNR loss is closer to 4.4 dB per halving.

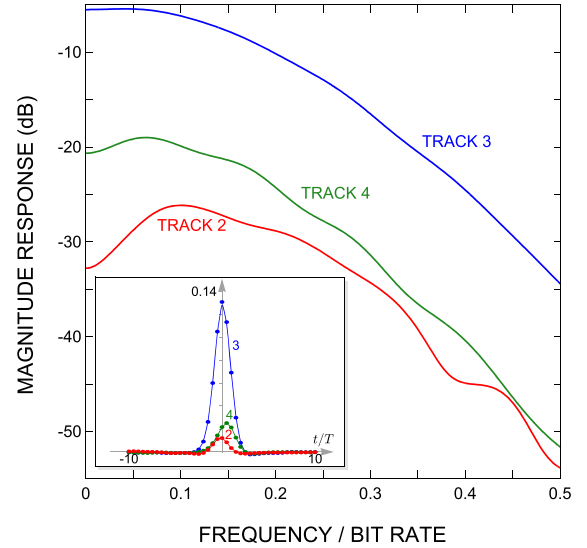


Fig. 2. Magnitude responses for a 70% width reader centered over track 3, for three different input tracks (2, 3, and 4). The track pitch is 16.1 nm, and the bit length is 7.3 nm. Inset: corresponding impulse responses in the time domain, spanning 20 b periods.

write $\mathbf{r} = \mathbf{h}\mathbf{A} + \mathbf{e}$, where $\mathbf{h} = [\mathbf{h}_1, \mathbf{h}_2, \mathbf{h}_3, \mathbf{h}_4, \mathbf{h}_5]$ is a long vector of concatenated impulse response vectors, and $\mathbf{A} = [\mathbf{A}_1^T, \mathbf{A}_2^T, \mathbf{A}_3^T, \mathbf{A}_4^T, \mathbf{A}_5^T]^T$ is a matrix of vertically stacked convolution matrices. The least-squares estimate for all five impulse responses is thus

$$\hat{\mathbf{h}} = \mathbf{r}\mathbf{A}^T(\mathbf{A}\mathbf{A}^T)^{-1}. \quad (1)$$

For example, in Fig. 2, we show the typical results of such a measurement for the case of a 70% width reader centered over track 3, when the track pitch is 16.1 nm and the bit length is 7.3 nm. The magnitude response for track 3 is roughly 15 dB stronger than those for the neighboring tracks (tracks 2 and 4). The corresponding impulse responses are shown in the inset, with time spanning 20 b periods. One may note how the low-frequency content of track 2 is damaged by the subsequent writing of track 3. Low frequencies have high demagnetizing fields and are susceptible to the stray fields from the head as the next track is written.

From the impulse response, we can estimate the signal level (or saturation level) in response to a long series of 1 b, or equivalently the dc gain, by summing all of the impulse response coefficients. In Fig. 3, we illustrate how the signal level changes as a function of the reader width, assuming that the reader is centered over the desired track, for track pitches ranging from 16.1 to 26.1 nm. The bit length is 7.3 nm. Signal level increases nearly linearly over a wide range of reader widths (a truly linear dependence is indicated by the dashed lines, for the sake of comparison). Although the reader geometry is scaled linearly, the resulting sensitivity function drops more rapidly for narrow readers.

The signal (saturation) level from a neighboring track to a reader centered on a different track can be used to quantify intertrack interference (ITI). In Fig. 4, we show the ITI as a function of reader position and reader width, assuming a 16.1 nm track pitch and a 7.3 nm bit length. As expected, wider readers are seen to increase both the desired signal level

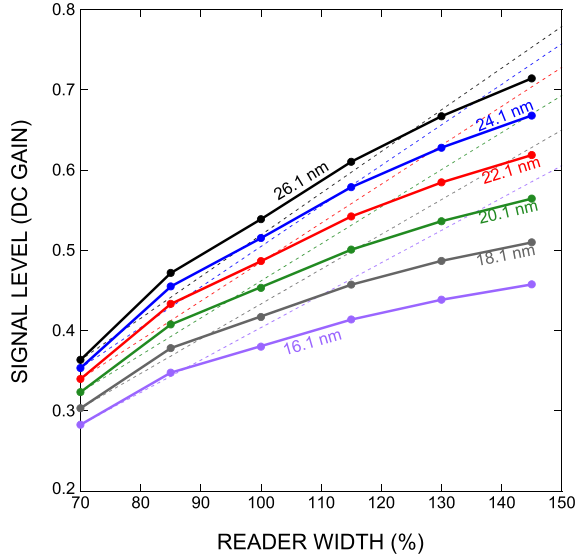


Fig. 3. Signal level for a centered reader versus reader width, for a bit length of 7.3 nm.

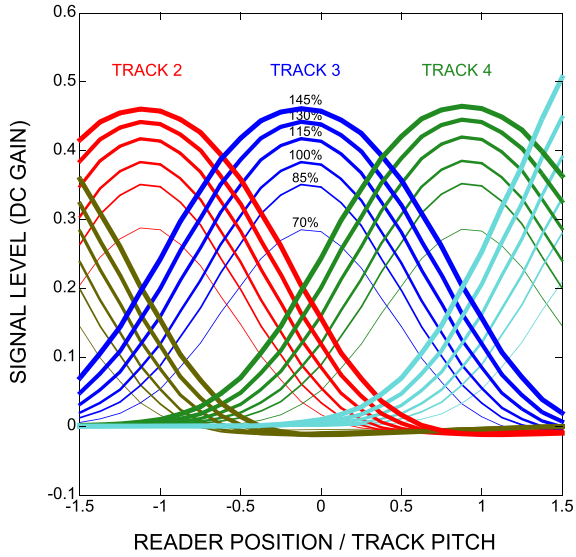


Fig. 4. ITI as quantified by signal level (dc gain) for 16.1 nm track pitch, 7.3 nm bit length, and different reader widths.

and the ITI signal level. Track 5 is wider than the others, because it is the last to be written (see Fig. 1) which explains its higher signal level in Fig. 4.

Nonlinear distortion in the form of nonlinear transition shift is to be expected, since the writing process did not include any precompensation of the transition positions. A truncated Volterra model for the noiseless readback waveform from an isolated track is [10], [11]

$$\begin{aligned}
 r(t) = & \sum_k a_k h(t - kT) \\
 & + \sum_k a_k a_{k-1} h^{(2)}(t - kT) \\
 & + \sum_k a_{k-1} a_k a_{k+1} h^{(3)}(t - kT)
 \end{aligned}$$

where $a_k \in \{\pm 1\}$ is the k th written bit on the track, T is the bit period, $h(t)$ is the (first-order) linear impulse response,

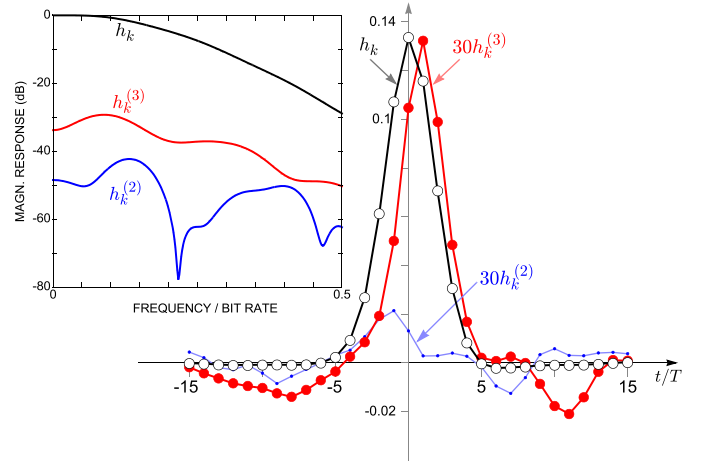


Fig. 5. Comparison of the linear impulse response h_k (open markers) and higher order nonlinear impulse responses (closed markers) for a 70% wide reader centered over track 3 and a track pitch of 16.1 nm. The third-order response $h_k^{(3)}$ is seen to have a similar shape as the linear impulse response, only weaker by a factor of 30. The second-order response is considerably weaker. Inset: corresponding magnitude responses.

$h^{(2)}(t)$ is the second-order nonlinear response for neighboring bits, and $h^{(3)}(t)$ is the third-order nonlinear response for three consecutive bits. This third-order nonlinearity captures the impact of nonlinear distortion in which the magnetic field from bit a_k influences the formation of the transition between a_k and a_{k+1} . The nonlinear responses can be estimated through (1), but where the convolution matrices are derived not from the written bits a_k but instead from the relevant product of bits [e.g., $a_k a_{k-1}$ for $h^{(2)}(t)$ and $a_{k-1} a_k a_{k+1}$ for $h^{(3)}(t)$]. A comparison of these three Volterra kernels is shown in Fig. 5, for the case of a 70% width reader centered over track 3, with a track pitch of 16.1 nm and a bit length of 7.3 nm. The oversampled linear impulse response h_k is seen to dominate by more than 30 dB. The oversampled third-order response $h_k^{(3)}$ is the next strongest; when scaled by a factor of 30, it shares nearly the same height and shape as the linear impulse response. The second-order response is significantly weaker.

Once the impulse responses to a given reader have been estimated, we can predict the corresponding sampled readback waveform by convolving the known bit sequences written on all five tracks with the corresponding linear impulse response estimates, or equivalently in terms of the notation of (1), according to $\hat{\mathbf{r}} = \hat{\mathbf{h}}\mathbf{A}$. Any error $\mathbf{e} = \mathbf{r} - \hat{\mathbf{r}}$ between this prediction and the actual samples (before adding electronic noise) can be attributed to media noise and nonlinear distortion, the latter being a much smaller contributor. If $\sigma_{\text{media}}^2 = \|\mathbf{e}\|^2/L$ denotes an estimate of the variance of this media noise, where L is the length of \mathbf{e} , and if H_0 denotes the dc gain, then the SNR (with respect to the dc gain) can be computed as $\text{SNR} = H_0^2 / (\sigma_{\text{media}}^2 + \sigma_e^2/2)$, where we use $\sigma_e = 0.04$ for the added electronic noise. Observe that this measure of SNR is independent of ITI, as might result from either an isolated track or for the case when ITI is perfectly canceled.

The dependence of SNR on reader width is shown in Fig. 6. The solid curves include the electronic noise, while the dashed curves have no electronic noise ($\sigma_e = 0$). In all cases, we see

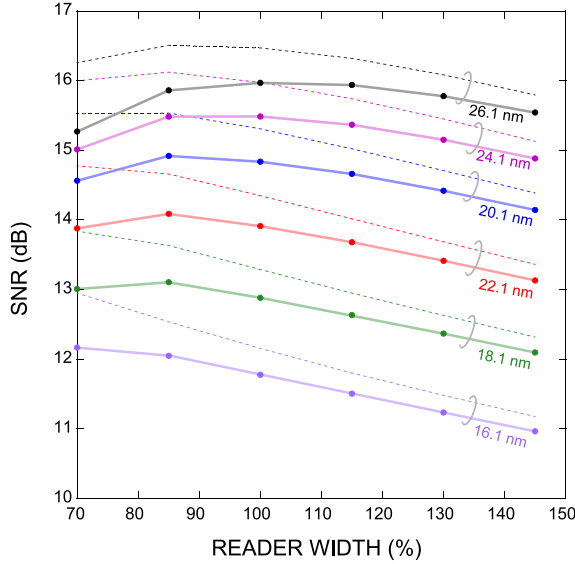


Fig. 6. SNR versus reader width, for a centered reader and a bit length of 7.3 nm. Dashed curves: no noise ($\sigma_e = 0$). Solid curves: electronic noise ($\sigma_e = 0.04$).

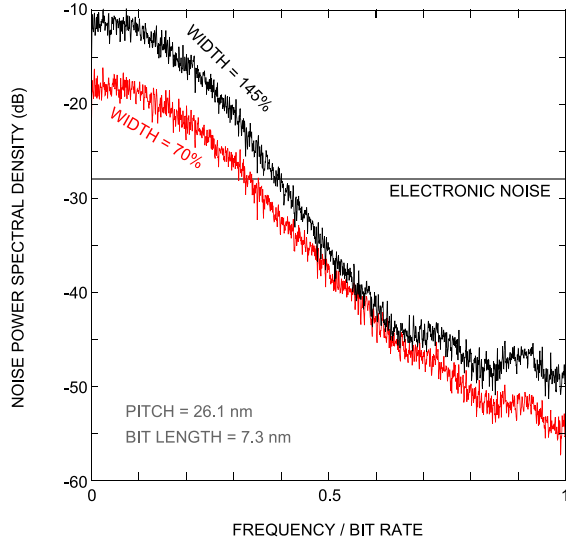


Fig. 7. Media noise power spectral densities for two different reader widths, assuming a centered reader, a track pitch of 26.1 nm, and a bit length of 7.3 nm. The electronic noise level is shown for comparison.

an optimum reader width that trades off the opposing goals of capturing as much desired signal energy (using a wide reader) and avoiding the media noise at the track edges (using a narrow reader).

The power-spectral density for the media noise $\mathbf{e} = \mathbf{r} - \hat{\mathbf{h}}\mathbf{A}$ is shown in Fig. 7 for a centered reader over a track with a pitch of 26.1 nm. The top curve is for a 145% reader width, and the bottom curve is for the 70% reader width. The spectrum of the media noise is clearly seen to be shaped by the reader response, in contrast to the spectrum of the electronic noise.

The media noise $\mathbf{e} = \mathbf{r} - \hat{\mathbf{h}}\mathbf{A}$ (1) is computed by subtracting the linear ISI and ITI contributions from the readback waveform. The variance of each media noise sample is time varying and data dependent. This time variance and data dependence are captured by an instantaneous measure

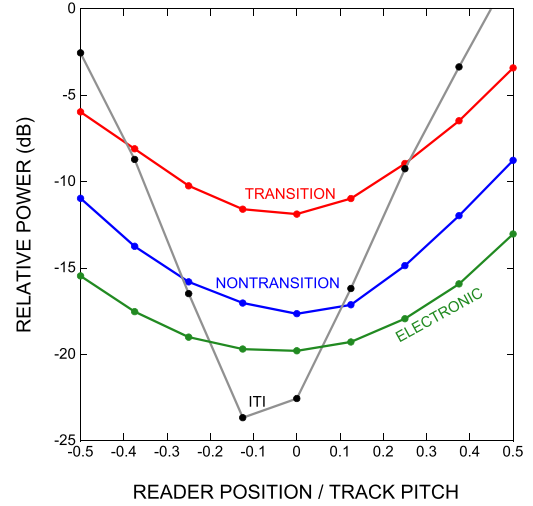


Fig. 8. Dependence of noise on crosstalk reader position.

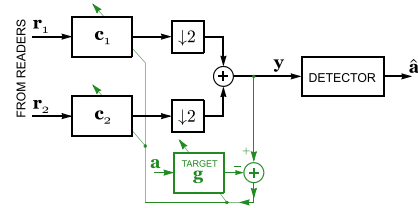


Fig. 9. Single-track detector preceded by a pair of fractionally spaced equalizers, whose outputs are downsampled and added. The equalizers and monic-constrained target are jointly designed to minimize mean-squared error.

$\sigma_{\text{media},k}^2$ of media noise variance at each time k , conditioned on knowledge of the written bits. Galbraith *et al.* [12] proposed the following linear model for this time-varying data-dependent variance:

$$\hat{\sigma}_{\text{media},k}^2 = \sigma_0^2 + \sum_i t_i w_{k-i}$$

where the first term σ_0^2 is independent of the presence of a transition, representing the nontransition media noise, and the second term represents the transition-dependent media noise, expressed in terms of the transition sequence $t_k = |a_k - a_{k+1}|/2 \in \{0, 1\}$ and the so-called transition noise response sequence w_k .

With $\{\sigma_{\text{media},k}^2\}$ measured experimentally, Galbraith *et al.* [12] proposed to estimate the parameters σ_0^2 and $\{w_k\}$ so as to minimize $\sum_k |\hat{\sigma}_{\text{media},k}^2 - \sigma_{\text{media},k}^2|^2$, and to use the resulting estimates to quantify the transition noise power and the nontransition noise power. Fig. 8 shows the sample results of this measurement technique for the case of a 70% width reader, a track pitch of 22.1 nm, and a bit length of 7.3 nm. Fig. 8 shows the relative power of four disturbances as a function of the crosstalk reader position: 1) the ITI power; 2) the transition noise power; 3) the nontransition noise power; and 4) the electronic noise power. All powers are normalized by the power of the desired signal for the main track, so that a value of 0 dB means that the noise power is equal to the signal power.

IV. MULTI-READER DETECTION

We limit consideration to single-track detectors of the form shown in Fig. 9. The two oversampled readback waveforms

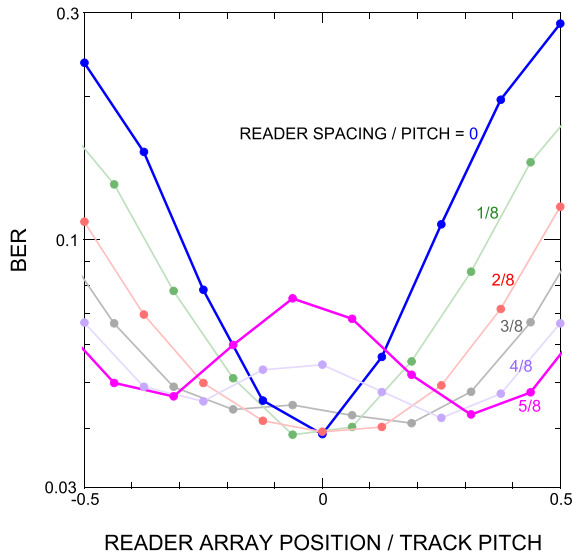


Fig. 10. Impact of spacing between two 70% width readers on the bathtub curve. The horizontal axis is the position of the array center (i.e., the midpoint between the two readers). The track pitch is 18.1 nm, and the bit length is 7.3 nm. Closely spaced readers yield the lowest BER, but wider spacing is more robust to misregistration.

from the two readers are separately equalized by a pair of fractionally spaced equalizers, each with N_c coefficients, and then added together. The pair of equalizers and the 1-D monic-constrained target $\mathbf{g} = [1, g_1, \dots, g_\mu]$ with memory μ are jointly optimized using standard techniques so as to minimize mean-squared error [13], so that the subsequent processing can use the conventional 1-D Viterbi [14] and Bahl, Cocke, Jelinek, and Raviv (BCJR) detectors [15].

The optimum spacing between two readers depends on many factors, but roughly boils down to a compromise between a desire to use a small spacing, so as to avoid the noise and ITI at the track edges, and a desire to use a large spacing, to reduce transition media noise through averaging, and to provide robustness to misregistration. In Fig. 10, we illustrate this tradeoff via a family of bathtub curves, for the case of two 70% width readers and a track pitch of 18.1 nm. Six curves are shown, for normalized reader spacings (normalized by the track pitch) ranging from zero to 5/8 in increments of 1/8. The narrowest bathtub curve corresponds to a zero crosstrack spacing; the two corresponding readback waveforms will thus have precisely the same media noise, differing only because the added electronic noise is independent. Slightly better bit-error rate (BER) performance at the bottom of the curve is achieved by a normalized spacing of 1/8. More significant, however, is the greater width of the resulting bathtub curve, making this configuration more robust to misregistration. Further increasing the spacing beyond 1/8 results in an even wider curve, albeit with a somewhat larger minimum value. If we were to choose the spacing to minimize the BER value at the bottom of the curve, ignoring the width of the curve, we would choose 1/8.

V. SYMMETRIC INFORMATION RATE

The BER after Viterbi detection is a useful performance metric when optimizing the multi-reader geometry for a given

track pitch and bit length, but it cannot be used to optimize the track pitch and bit length parameters themselves. Here, we propose a more comprehensive metric that can be used to simultaneously optimize all parameters. An ideal optimization metric would be the Shannon capacity, since it would upper bound the areal density for any practical system. Instead, because the Shannon capacity is not known for this channel, we propose to use the symmetric information rate (SIR) between the input sequence \mathbf{a} of written bits on the home track and the output sequence \mathbf{y} after the equalizer(s). The SIR is the mutual information rate $I(\mathbf{a}; \mathbf{y})$ between \mathbf{a} and \mathbf{y} under the constraint that the written bits are independent and uniformly distributed (i.i.d.) random variables, namely

$$\text{SIR} = h(\mathbf{y}) - h(\mathbf{y}|\mathbf{a}) \quad (2)$$

where $h(\mathbf{y})$ is the entropy rate of the equalizer output and $h(\mathbf{y}|\mathbf{a})$ is the conditional entropy rate of the output, given \mathbf{a} .

The units of SIR are information bits, and can be interpreted as a bound on the average number of user bits per written bit. Therefore, the areal density (in units of bits per grain) can be computed as SIR/G , where G is the average number of grains per written bit, and can be computed from the track pitch, bit length, and grain density (for example, a track pitch of 16.1 nm, a bit length of 7.3 nm, and 22 Tgr/in² leads to $G = 4.01$ grains/written bit). Like Shannon capacity, the SIR is a property of the communication channel itself, and is not tied to any particular coding scheme or decoding strategy. The SIR thus provides a useful benchmark for achievable storage densities for systems that use single-track detection with multiple readers.

Let us write the equalizer output as

$$\mathbf{y} = \mathbf{s}(\mathbf{a}) + \mathbf{n}(\mathbf{a})$$

where without loss of generality we define the k th component of $\mathbf{s}(\mathbf{a})$ as the linear convolution $s_k = \sum_{i=0}^{\mu} g_i a_{k-i}$, where $\{g_0, \dots, g_\mu\}$ are the target coefficients; any nonlinearities or other effects can then be lumped into the additive signal-dependent noise, defined as $\mathbf{n}(\mathbf{a}) \triangleq \mathbf{y} - \mathbf{s}(\mathbf{a})$. Suppose the noise is data-dependent order- L autoregressive (AR) and Gaussian of the form [16]

$$n_k(\mathbf{a}) = \sigma_k(\mathbf{a}_k)u_k + \sum_{i=1}^L p_{i,k}(\mathbf{a}_k)n_{k-i} \quad (3)$$

where $\{u_k\}$ is an i.i.d. sequence of zero-mean unit-variance Gaussian random variables and $\sigma_k(\mathbf{a}_k)$ and $\mathbf{p}_k(\mathbf{a}_k) = [p_{1,k}(\mathbf{a}_k), \dots, p_{L,k}(\mathbf{a}_k)]$ are the data-dependent time-varying AR parameters that depend at time k only on the $\mu + 1$ written bits $\mathbf{a}_k \triangleq [a_k \dots a_{k-\mu}]$. Applying the noise of (3) to a time-varying linear predictor of the form $\hat{n}_k = \sum_{i=1}^L p_{i,k}(\mathbf{a}_k)n_{k-i}$ with knowledge of \mathbf{a} would then lead to an uncorrelated prediction error sequence $e_k = n_k - \hat{n}_k = \sigma_k(\mathbf{a}_k)u_k$.

We now examine how to compute the second of the two terms in (2), namely, $h(\mathbf{y}|\mathbf{a})$. When the AR model of (3) is exact, the conditional entropy $h(\mathbf{y}|\mathbf{a})$ can be computed exactly. Considering that $h(\mathbf{y}|\mathbf{a})$ is a measure of uncertainty in \mathbf{y} given knowledge of \mathbf{a} , and further that knowledge of \mathbf{a}

and the AR parameters enables us to extract \mathbf{e} through linear prediction, it follows that the conditional entropy reduces to:

$$h(\mathbf{y}|\mathbf{a}) = h(\mathbf{e}) = \frac{1}{2} \log_2(2\pi e\bar{\sigma}^2)$$

where $\bar{\sigma}^2 = 2^{E(\log_2 \sigma_k^2(\mathbf{a}_k))}$. This further reduces to $h(\mathbf{n}) = (1/2) \log_2(2\pi e\sigma^2)$, as expected, in the special case when the noise \mathbf{n} is additive white Gaussian noise and independent of \mathbf{a} .

When the noise is AR according to (3), the first term $h(\mathbf{y})$ in (2), the entropy of the equalizer output, can also be computed exactly; it can be computed using the forward recursion of the BCJR algorithm, as explained in [17], which operates on a $2^{\mu+1+L}$ -state trellis.

In the spirit of [18], data-dependent noise prediction can still be used to estimate the conditional entropy $h(\mathbf{y}|\mathbf{a})$, and the forward recursion of BCJR can still be used to estimate $h(\mathbf{y})$, even when the noise does not strictly follow the AR model of (3). Strategies for empirically estimating $\sigma_k(\mathbf{a}_k)$ and $\mathbf{p}_k(\mathbf{a}_k)$ are discussed in [18].

VI. OPTIMIZATION RESULTS

We first assume a bit length of 7.3 nm and optimize all other parameters. We then fix these remaining parameters and optimize bit length. In particular, for the 7.3 nm bit length and every track pitch and reader geometry, the corresponding pair of readback waveforms was processed according to Section IV, and both the SIR and the BER computed. An exhaustive search over all possible candidate geometries was then performed. A similar exhaustive search was also performed for a single-reader system.

Results are shown in Fig. 11, where we plot BER after a standard four-state Viterbi detection (without noise prediction) versus track pitch. Every parameter of the system (bit geometry, reader geometry, equalizer, and target) is optimized separately for each point in the curves so as to minimize the resulting BER. The two-reader system is seen to offer up to an 11% increase in areal density over the single-reader system.

A similar search was performed so as to maximize the SIR in units of bits per grain, rather than to minimize BER. The results are shown in Fig. 12, where we plot the optimized areal density versus track pitch. The units on the left are Tb/in^2 , while the units on the right are bits/grain. As before, every parameter of the system (bit geometry, reader geometry, equalizer, and target) is optimized separately for each point in the curves so as to maximize the areal density. A maximum areal density of at 4.8 Tb/in^2 (or 0.22 b/grain) is achieved at a track pitch of 16.1 nm, with the reader widths of 23.9 and 14.6 nm and a center spacing of 2 nm. The corresponding code rate is 0.79. Compared with an optimized single-reader system, the second reader provides a 5% increase in areal density.

Comparing Figs. 11 and 12, we see what appears to be a contradictory trend. In terms of BER, the gain from the second reader increases with track pitch, while in terms of SIR, the gain decreases with track pitch. This can be explained in part by the nonlinear relation between BER and capacity.

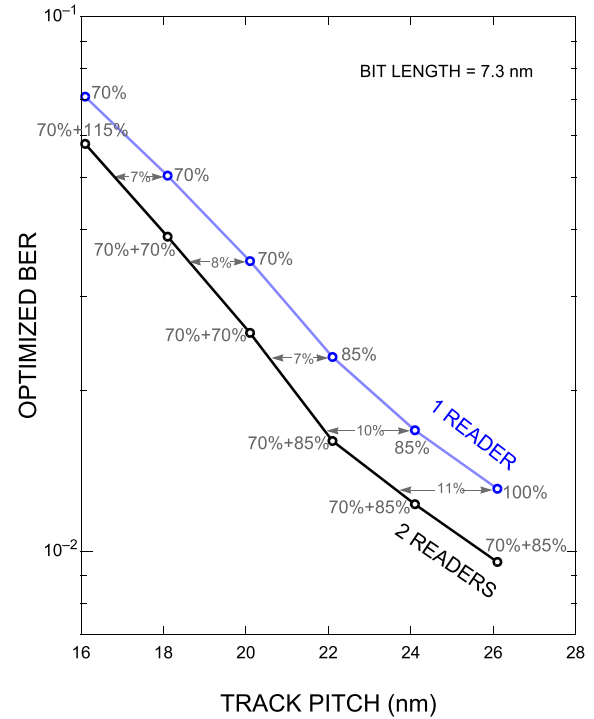


Fig. 11. Optimized BER versus track pitch for a bit length of 7.3 nm. At each point, the equalizers, target, reader widths, reader spacing, and position are optimized to minimize BER. The optimum reader widths are indicated at each point.

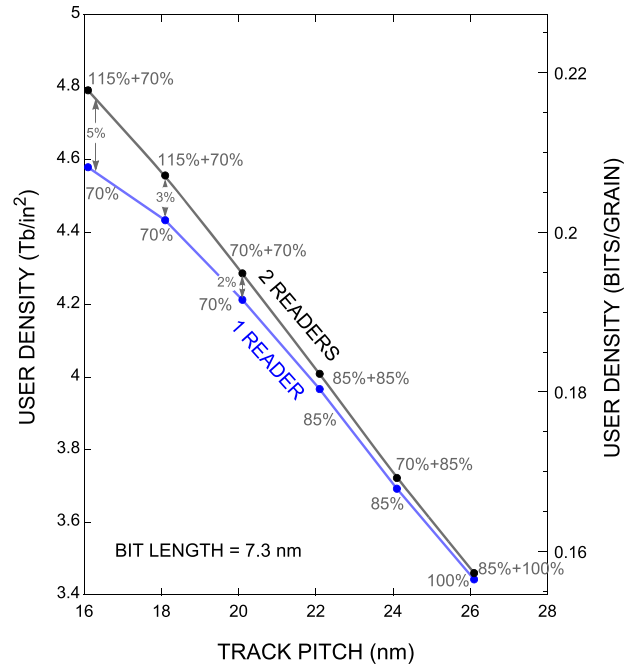


Fig. 12. Optimized areal density versus track pitch, as predicted by SIR, for a bit length of 7.3 nm. The units on the left axis are Tb/in^2 , while the units on the right are user bits per grain.

For example, consider the impact of halving the BER on a binary-symmetric channel whose crossover probability is equal to BER. The impact is large at low SNR (as might arise with low track pitch); for example, cutting the BER from 0.1 to 0.05 increases the capacity by over 34%. In contrast, the impact

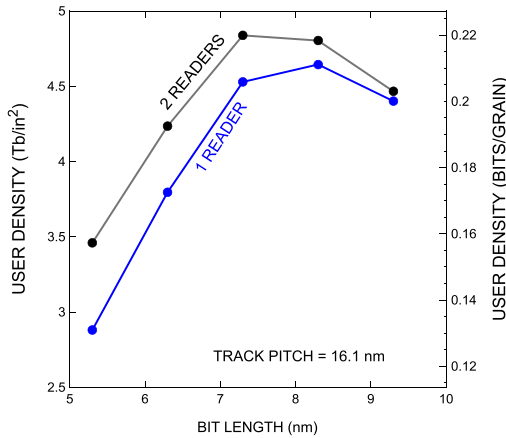


Fig. 13. Areal density as a function of bit length, as predicted by SIR. The reader geometry was fixed at two 70% wide readers with a 1/8-pitch spacing, and the track pitch is 16.1 nm.

is significantly less at high SNR: cutting the BER from 10^{-3} to 0.5×10^{-3} increases the capacity by $<1\%$.

We next examine performance as a function of bit length. Up to now, we have added the same amount of electronic noise to each readback waveform, regardless of the reader width. But when varying the bit length while keeping the rotational speed of the medium fixed, we must scale the noise standard deviation to account for the change in bit rate. In particular, to be consistent with the choice of $\sigma_e = 0.04$ when the bit length was $L_0 = 7.3$ nm, the electronic noise standard deviation value as a function of bit length L_b is $\sigma_e = 0.04(L_0/L_b)^{1/2}$. With the track pitch fixed at its optimal value (16.1 nm), and while keeping the reader geometry fixed at two 70% wide readers with a 1/8-pitch spacing, we computed the SIR as a function of bit length. The results are shown in Fig. 13 for the case of one and two readers. The one-reader system achieves a maximum areal density at 8.3 nm, while the two-reader system achieves a maximum at 7.3 nm.

VII. CONCLUSION

The large database of simulated waveforms was used to perform a comprehensive exhaustive search for optimizing the geometry of multiple readers so as to maximize density. Moving from one to two readers was shown to increase the maximal areal density by 5%. Further gains in areal density can be expected by relaxing the constraints of the single-track reader architecture considered here, e.g., by considering multi-track detectors based on a joint Viterbi algorithm, by employing modulation codes controlling both downtrack and crosstrack transitions, and by employing crosstrack media-noise processing, such as data-dependent noise prediction. Our optimization results are limited not only by the fact that they were based on zero skew and misregistration, but also by the limited range of track pitches and bit lengths considered. A broader optimization criterion that accounts for both skew and track misregistration will likely lead to different optimization results.

ACKNOWLEDGMENT

This work was supported in part by Storage Research Consortium, Japan, in part by IDEMA ASTC, USA, and in part by the Directorate for Biological Sciences through the National Science Foundation under Grant CCF-1314147. The authors would like to thank R. Wood and H. Mutoh for the guidance and support.

REFERENCES

- [1] R. Wood, M. Williams, A. Kavcic, and J. Miles, "The feasibility of magnetic recording at 10 terabits per square inch on conventional media," *IEEE Trans. Magn.*, vol. 45, no. 2, pp. 917–923, Feb. 2009.
- [2] ASTC. (2014). *ASTC Technology Roadmap: 2014 v8*. [Online]. Available: <http://www.idema.org/>
- [3] S. Dahandeh, M. F. Erden, and R. Wood, "Areal-density gains and technology roadmap for two-dimensional magnetic recording," in *Proc. TMRC*, Aug. 2015, p. Paper F1.
- [4] R. Wood, R. Galbraith, and J. Coker, "2-D magnetic recording: Progress and evolution," *IEEE Trans. Magn.*, vol. 51, no. 4, Apr. 2015, Art. ID 3100607.
- [5] M. Igarashi, M. Hara, A. Nakamura, and Y. Sugita, "Micromagnetic simulation of magnetic cluster, thermal activation volume, and medium noise in perpendicular recording media," *IEEE Trans. Magn.*, vol. 39, no. 4, pp. 1897–1901, Jul. 2003.
- [6] B. Vasić *et al.*, "A study of TDMR signal processing opportunities based on quasi-micromagnetic simulations," *IEEE Trans. Magn.*, vol. 51, no. 4, Apr. 2015, Art. ID 9401307.
- [7] M. Yamashita *et al.*, "Modeling of writing process for two-dimensional magnetic recording and performance evaluation of two-dimensional neural network equalizer," *IEEE Trans. Magn.*, vol. 48, no. 11, pp. 4586–4589, Nov. 2012.
- [8] Y. Yamashita, Y. Okamoto, Y. Nakamura, H. Osawa, S. J. Greaves, and H. Muraoka, "Performance evaluation of neuro-ITI canceller using a modified writing process for TDMR," *IEICE Trans. Electron.*, vol. E96-C, no. 12, pp. 1504–1507, Dec. 2013.
- [9] Y. Kanai, Y. Jinbo, T. Tsukamoto, S. J. Greaves, K. Yoshida, and H. Muraoka, "Finite-element and micromagnetic modeling of write heads for shingled recording," *IEEE Trans. Magn.*, vol. 46, no. 3, pp. 715–721, Mar. 2010.
- [10] D. Palmer, P. Ziperovich, R. Wood, and T. D. Howell, "Identification of nonlinear write effects using pseudorandom sequences," *IEEE Trans. Magn.*, vol. 23, no. 5, pp. 2377–2379, Sep. 1987.
- [11] R. Hermann, "Volterra modeling of digital magnetic saturation recording channels," *IEEE Trans. Magn.*, vol. 26, no. 5, pp. 2125–2127, Sep. 1990.
- [12] R. Galbraith, W. Hanson, B. Lengsfeld, T. Oenning, J. Park, and M. Salo, "Noise characterization in high-areal density perpendicular and shingled magnetic recording," *IEEE Trans. Magn.*, vol. 50, no. 3, Mar. 2014, Art. ID 3200707.
- [13] J. Moon and W. Zeng, "Equalization for maximum likelihood detectors," *IEEE Trans. Magn.*, vol. 31, no. 2, pp. 1083–1088, Mar. 1995.
- [14] G. D. Forney, Jr., "The Viterbi algorithm," *Proc. IEEE*, vol. 61, no. 3, pp. 268–278, Mar. 1973.
- [15] L. R. Bahl, J. Cocke, F. Jelinek, and J. Raviv, "Optimal decoding of linear codes for minimizing symbol error rate (Corresp.)," *IEEE Trans. Inf. Theory*, vol. 20, no. 2, pp. 284–287, Mar. 1974.
- [16] A. Kavčić and J. M. F. Moura, "The Viterbi algorithm and Markov noise memory," *IEEE Trans. Inf. Theory*, vol. 46, no. 1, pp. 291–301, Jan. 2000. [Online]. Available: <http://dx.doi.org/10.1109/18.817531>
- [17] D. M. Arnold, H.-A. Loeliger, P. O. Vontobel, A. Kavčić, and W. Zeng, "Simulation-based computation of information rates for channels with memory," *IEEE Trans. Inf. Theory*, vol. 52, no. 8, pp. 3498–3508, Aug. 2006.
- [18] J. Moon and J. Park, "Pattern-dependent noise prediction in signal-dependent noise," *IEEE J. Sel. Areas Commun.*, vol. 19, no. 4, pp. 730–743, Apr. 2001. [Online]. Available: <http://dx.doi.org/10.1109/49.920181>